Temperature dependence of the inverse photoemission from copper surfaces

R. Schneider, H. Dürr, Th. Fauster, and V. Dose
Max-Planck-Institut für Plasmaphysik, EURATOM Association, Boltzmannstrasse 2, D-8046 Garching/München, Federal Republic of Germany
(Received 29 January 1990)

The temperature dependence of the intensity of inverse photoemission transitions into bulk and surface states has been studied on Cu(100), (110), and (111) surfaces. The temperature dependence is strongly influenced by multiple-scattering effects. For Cu(100) and (111) it can be fitted very well with a Debye-Waller law where the mean-square displacements of the surface atoms increase linearly with temperature. For Cu(110) we find an enhancement of the mean-square displacements above 400 K in agreement with surface-sensitive scattering experiments. Through the comparison of a given bulk transition on different surfaces, we find a strong influence of surface vibrations on the intensities of bulk transitions. A classification of the temperature dependence of the investigated bulk transitions is attempted in a two-band model, in a nearly-free-electron model, and in the one-step model of inverse photoemission incorporating bulk and surface phonons. The results are not quite satisfying, although they seem to show the right trend: the temperature dependence is stronger the higher the energy is. The temperature dependence of the surface-state transitions depends on their character. Transitions into image-potential surface states are temperature independent. Transitions into crystal-induced surface states respond to temperature changes. Transitions into states that are located in the same band gap and have nearly the same relative position in it show the same temperature dependence. The temperature dependence gets smaller the more bulklike the surface state gets.

I. INTRODUCTION

The study of electronic states at surfaces has reached a very high standard in recent years. The agreement between the experimentally measured dispersion for bulk and surface states and *ab initio* calculations is very good for the transition metals, although the measured intensities may differ from the calculated ones.

Until now the temperature effects in photoemission (PES) and inverse photoemission (IPE) are not satisfactorily understood and only a small number of papers have dealt with this subject. The experimentally observed effects are peak shifts due to the lattice expansion with increasing temperature,[1] peak broadening due to an increased probability for indirect phonon-assisted transitions,[2] which leads to a background increasing with temperature[3,4] and a reduction of the intensity of direct transitions.[5,6] Moreover, structural changes of the surface with temperature can affect the observed spectra. These structural changes can be purely geometrical in the case of reconstruction,[7] or magnetic in the case of ferromagnets.[8]

In IPE the reduction of the intensity of direct transitions is usually the most notable effect.[5] In spin-polarized IPE, temperature-dependent studies are important for the study of magnetic phase transitions and the nature of magnetic ordering in band ferromagnets.[8] An understanding of the nonmagnetic temperature effects is a necessary prerequisite for a discussion of the magnetic effects.

In this work we measured the temperature dependence of IPE transitions into various surface and bulk states for copper. Since the band structure of copper is well understood[5,9,10] copper provides a good test system for the study of temperature effects in IPE. In Sec. II the results of our IPE measurements at room temperature will be summarized for the three low-index copper surfaces (100), (110), and (111). The experimental data will be compared with results of a combined interpolation-scheme calculation. This allows the identification of the character of the observed bulk transitions, which will be shown to be important for the temperature dependence. The comparison of an identical transition observed on different surfaces allows a triangulation of this transition. The experimental data of the temperature dependence of transitions into various surface and bulk states for Cu(100), (110), and (111) are presented in Sec. III. Though theoretical models exist for all the experimentally observed temperature effects, the agreement is at best only qualitative in most cases.[1,11,12] The main reason is the enormous complexity of the multiple-scattering theories of PES, which makes a realistic treatment of a vibrating lattice intractable. Therefore, we try to compare empirical rules extracted from an extended experimental data basis with theoretical predictions for the temperature effects in photoemission spectroscopies. The important question of whether bulk or surface vibrations are responsible for the observed temperature effects is resolved with the help of a triangulation experiment: The temperature dependence of a given bulk direct transition is measured on two different surfaces. From this, we can separate surface-specific effects from the influence of bulk effects. We find that the temperature dependence of bulk transitions is dominated by surface vibrations. For bulk

electronic transitions we calculate, within a Debye-Waller model, mean-square displacements which compare well with results from scattering experiments, which probe only the top surface layer, thus supporting the outcome of the triangulation experiment. In this section we finally discuss the temperature effects on surface states. For a theoretical interpretation of our experimental results we identify the observed direct transitions into bulk states as transitions between nearly-free-electron (NFE) bands. Therefore, in Sec. IV we discuss the temperature effects in the two-band model and the NFE theory. In Sec. V the temperature effects are introduced into the one-step model, following the ideas of Larsson and Pendry[12] and using the results of phonon slab calculations. We summarize our results in Sec. VI.

II. RESULTS FOR CU(100), (110), AND (111) AT ROOM TEMPERATURE

In this section we will focus on the identification of the character of the bulk transitions and on the triangulation of a bulk transition from different surfaces. These data are important for the interpretation of the temperature-dependent results of Sec. III.

The IPE experiments used a Geiger-Müller counter with iodine filling and a CaF_2 entrance window that performs as a band-pass detector for photons of 9.6 eV energy.[13] The electron gun with BaO cathode was mounted on a rotatable platform, which allows a polarization analysis of the measured transitions.[14] The samples were aligned within 0.5° relative to the rotation axes of the manipulator as checked by ion scattering.[15] The normal incidence of the electrons has been determined by the dispersion of the IPE peaks and by total current spectroscopy[16] with an error of about 0.5°.

The IPE results for bulk transitions for the three low-index copper surfaces Cu(100), (110), and (111) have been extensively discussed in detail in previous studies.[5] Our experiments extended the $k_{\parallel}$ range and we measured for different photon detection angles to determine the polarization. For the identification of the character of the bulk transitions we compare the measured $E(k_{\parallel})$ curves with the results of a combined interpolation-scheme calculation[17] for the two mirror planes ΓXUL and ΓXWK. The combined interpolation scheme was fit at high-symmetry points to a self-consistent band-structure calculation of Bross *et al.*[18] In Fig. 1 the k-space location of the possible transitions with a photon energy of 9.6 eV from even initial states into final states in the energy range -1 to 8 eV in the two mirror planes can be seen. The two mirror planes are plotted in one figure by matching the two mirror planes at the ΓX line. Transitions from odd initial states have been omitted, because the initial-state coupling to the vacuum must always be even under reflection, with respect to the mirror plane.[19] The arrows in Fig. 1 indicate the direction of the surface normals. The different symbols belong to transitions between different bands, characterized by the difference of the dominant plane-wave components of the initial and final state. The symbols will be discussed later when the experimental observed data are compared with these predicted transitions. The transition matrix elements for photoemission are generally believed to be determined by the dipole operator $\mathbf{A}\cdot\mathbf{p}$,[20] the scalar product of the vector potential $\mathbf{A}$ and the momentum operator $\mathbf{p}$. For our photon-energy $\hbar\omega$ of 9.6 eV the vector potential can be assumed to be constant[21] and the transition matrix element is determined by the momentum matrix element. Within a simple two-band model[22] the momentum matrix element $\mathbf{p}$ is determined by the exchanged reciprocal-lattice vector $\mathbf{G}$, which is the difference between the initial-state reciprocal-lattice vector $\mathbf{G}_i$ and the final-state reciprocal-lattice vector $\mathbf{G}_f$,

$$\mathbf{p}=\mathbf{G}\mathbf{V}_{\mathbf{G}}/\omega \ . \tag{1}$$

$\mathbf{V}_{\mathbf{G}}$ is the Fourier component of the crystal potential for the reciprocal-lattice vector $\mathbf{G}$, which mediates the transition between the two free-electron-like sp bands. The size of the symbols is scaled with the square of the calculated dipole matrix element. The intensity changes of the transitions characterized by the same exchanged reciprocal-lattice vector indicate the inadequacy of the two-band model, where one would expect from Eq. (1) equal intensities for these transitions. The transition marked with a diamond is dominating and characterized by an exchanged lattice vector of (200). All the other transitions have much smaller transition matrix elements.

The possible transitions shown in Fig. 1 frequently run parallel to zone boundaries, as expected from the two-band model,[22] because within this model the isochromat surface should be a plane in $\mathbf{k}$-space

$$2\mathbf{k}\cdot\mathbf{G}=(2m/\hbar^2)[(\hbar\omega)^2-\mathbf{V}_{\mathbf{G}}^2]^{1/2}-\mathbf{G}^2 \ . \tag{2}$$

In Figs. 2–4 the data from our measurements on Cu(100), (110), and (111) for the bulk transitions are

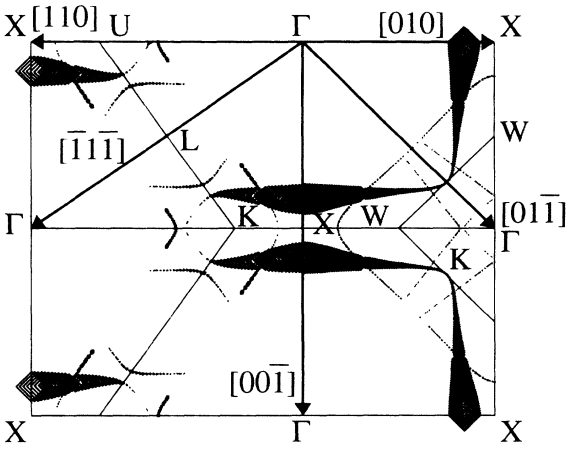

FIG. 1. Location of the possible transitions with photon energy of 9.6 eV from even initial states into final states in the energy range -1–8 eV in the two mirror planes of copper. The arrows indicate the directions of the surface normals. The different symbols belong to transitions between different bands characterized by the dominant plane-wave component of the wave function of the initial and final state $\mathbf{G}_i$ and $\mathbf{G}_f$ (in units of π/a). The size of the symbols is scaled with the square of the calculated matrix elements.

shown in $E(k_{\parallel})$ diagrams as solid symbols with error bars. Transitions into surface states are shown as open symbols with error bars. The transitions which have been measured subsequently as a function of temperature are marked with large squares. The size of the symbols indicates the intensity of the transition. To facilitate the identification of the surface states the band gaps of the projected bulk band structure are shown as grey shaded areas in Figs. 2–4. First, we will discuss the bulk transitions. The symbol gives their character, as extracted from the comparison with the calculated transitions, which are shown by the open symbols without error bars corresponding to Fig. 1. The dominating transition, characterized by an exchanged lattice vector of (200), is the transition marked with a diamond. Three other types of bulk transitions are observed: The triangle oriented to the right is a symbol for a transition characterized by an exchanged lattice vector of (200). The triangles pointing to the left and down are transitions characterized by an exchanged lattice vector of (111). Although their transition matrix elements are small compared with the dominating transition marked as a diamond (see Figs. 1–4) these transitions become visible in the experimental data due to initial-state effects, which will be discussed later. All the other predicted bulk transitions are characterized by an exchanged lattice vector of (111) and are not observed in the experiment. We also checked the expected dipole orientation of the experimentally observed transitions by comparing the results for different photon take-off angles and found a good agreement between theory and experiment as reported previously for Cu(100).[14] The dipole orientation is a test of the transition matrix elements and, consequently, of the wave functions. The good agreement between calculation and experiment in the dispersion, the intensities, and the dipole orientation prove the correct identification of the bulk transitions.

Additionally, the band gaps of the projected bulk band structure are shown as grey shaded areas. The transitions into surface states are marked as open symbols with error bars. For the discussion of surface-specific effects, bulk transitions, which can be triangulated, are very useful.[23] The main bulk transition shown as diamonds

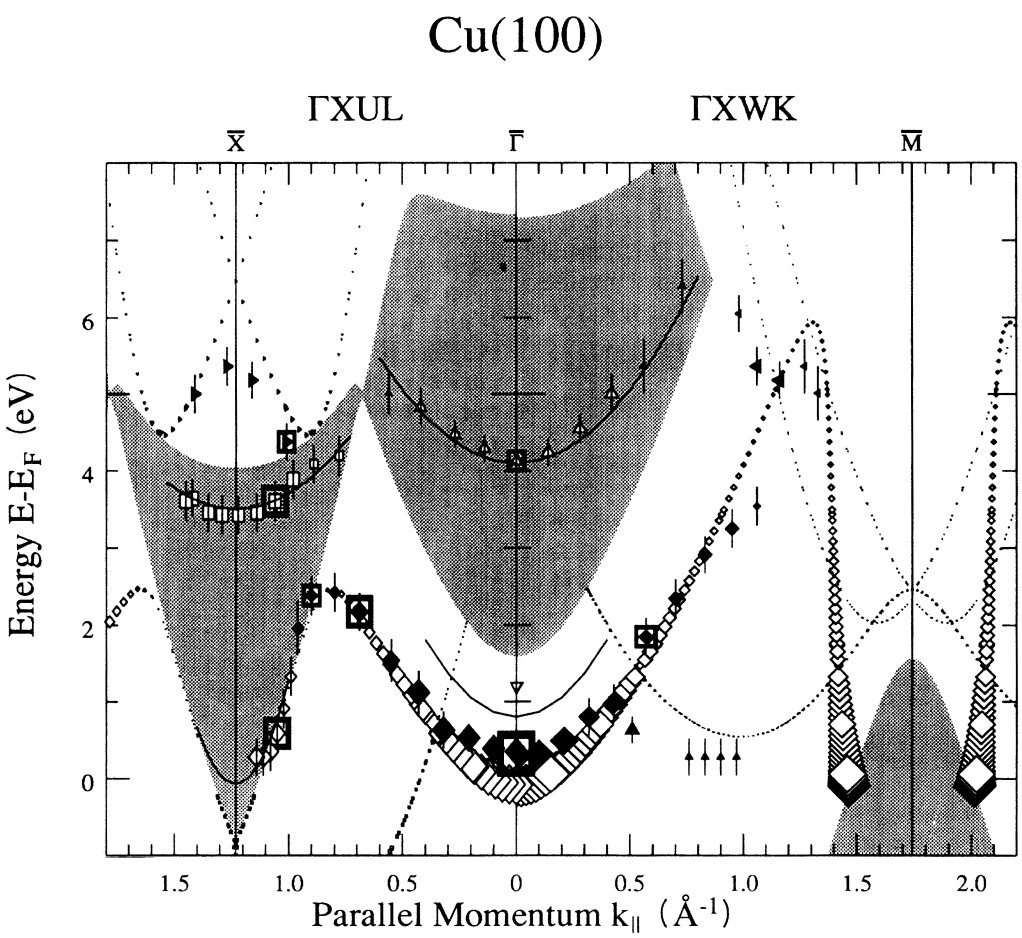

FIG. 2. $E(k_{\parallel})$ diagram for Cu(100). The calculated transitions are shown by the open symbols without error bars corresponding to Fig. 1. The data from our measurements for bulk transitions are shown as solid symbols with error bars. The size of the symbols indicates the intensity of the transition. The symbols of the measured bulk transitions were chosen to correspond to the calculated transitions. The band gaps of the projected bulk band structure are shown as grey shaded areas. The data from our measurements for transitions into surface states are marked as open symbols with error bars. The dispersion of the surface states is indicated by the parabolas.

should be seen on all three surfaces. It has for Cu(100) a high intensity only close to normal incidence.[14] In the ΓXUL mirror plane near to the zone boundary it runs close to the gap and transforms into a surface state.[24] On Cu(110) it can be seen with higher intensity only close to the gap in the ΓKWX mirror plane near the zone boundary.[25] For Cu(111) it occurs in the spectra close to the Fermi level.[5] In this region it can also be influenced by other possible transitions. For higher $k_{\parallel}$ for Cu(111) at about 1.3 Å^{-1} and 2–3 eV a structure can be seen in the experimental data, which might also be this transition. The position close to the gap also makes this a candidate for a surface state. These states will be discussed later.

The coupling of the incoming electron to the initial state can change the observed intensity compared to the expected calculated intensity. For the transitions marked as triangles in Figs. 2–4, e.g., in the case of Cu(100) in the ΓXUL mirror plane for the bulk transition close to the zone boundary at about 5 eV (Fig. 2), the coupling probability for the incoming electron is higher compared with the dominating transition marked as a diamond with higher transition matrix elements but smaller coupling probabilities. This enhances the intensity of these transitions compared to the predicted value and makes them experimentally observable.

At $\bar{\Gamma}$ for Cu(110) the omission of the odd initial states can be seen from the fact that some of the calculated curves do not appear in both mirror planes (Fig. 3). This effect of the coupling of the incoming electron is in agreement with experiment, which observes no direct transition for normal incidence for Cu(110).

For Cu(111) this initial-state effect is the reason that the $\bar{\Gamma}\bar{M}$ and the $\bar{\Gamma}\bar{M}'$ direction are no longer identical, although for energies below 8 eV only small intensity asymmetries can be seen (Fig. 4).

The surface states, lying in or close to the band gaps, measured with IPE for the three copper surfaces (100), (110) and (111) (Refs. 5, 25, and 26–30) can be grouped into two classes. The barrier-induced surface states are produced by the long-range image potential. They form a Rydberg series close to the vacuum energy.[31] The wave functions associated with these states protrude far into the vacuum and their probability density peaks well outside the solid. The crystal-induced surface states depend on the potential at and near the surface. The probability density of the associated wave functions peaks in the surface plane correspondingly.[31] The parabolas in Figs. 2–4 indicate the dispersion of the surface states. The barrier-induced surface states on Cu(100) and (111) close to normal incidence at $\bar{\Gamma}$ at 4.1 and 4.5 eV have been discussed in the literature before.[5] Our data agree well with the previously published results. For Cu(100) we see a crystal-induced surface state as a shoulder at (1.2 ± 0.3) eV, which cannot be resolved from the intense bulk transition at higher $k_{\parallel}$. This energy at $\bar{\Gamma}$ agrees well with the results of Hulbert *et al.*,[32] who measured the dispersion of

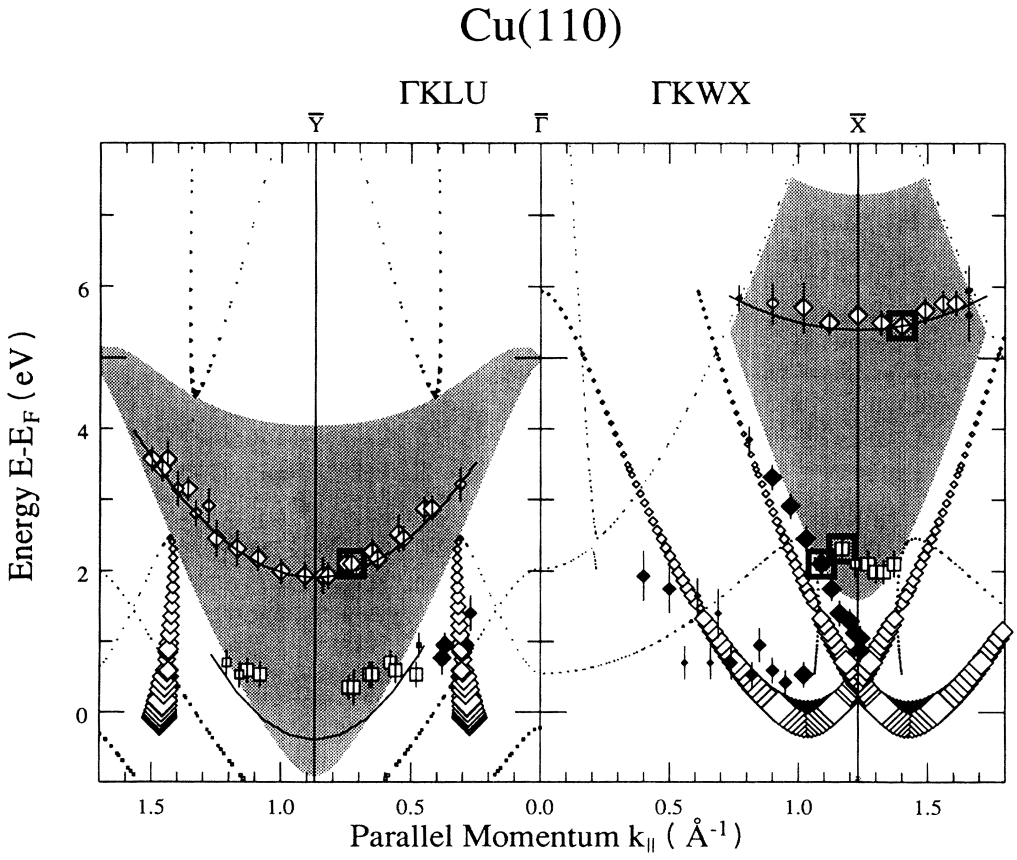

FIG. 3. $E(k_{\parallel})$ diagram for Cu(110). For an explanation see Fig. 2.

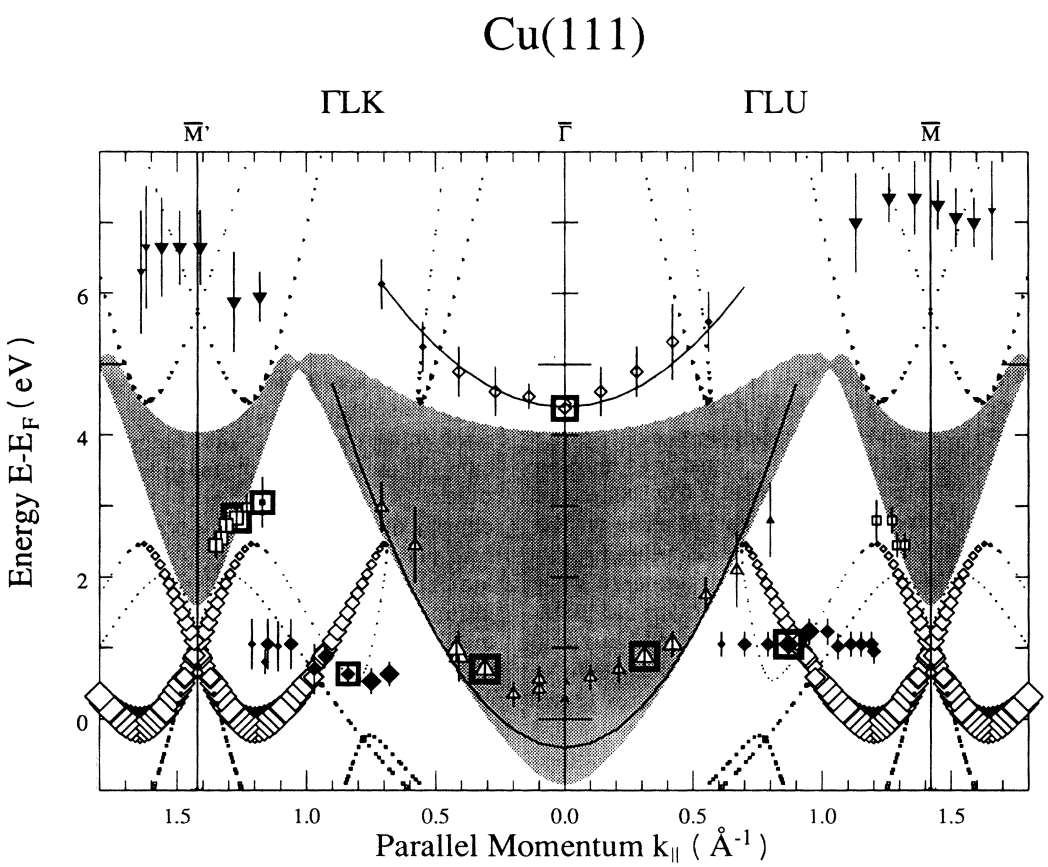

FIG. 4. $E(k_{\parallel})$ diagram for Cu(111). For an explanation see Fig. 2.

this surface state with a monochromator for a constant initial-state energy and variable photon energy and found at $\bar{\Gamma}$ an energy of 0.8 eV and an effective mass of 0.4 close to $\bar{\Gamma}$ and 0.6 at higher $k_{\parallel}$. This is shown as the parabola in the bulk region. In the ΓXUL mirror plane our results for the two crystal-induced surface states at $\bar{X}$ agree well with results of Donath *et al.*[24] We extended their $k_{\parallel}$ range and therefore measured the dispersion of the surface state close to the Fermi energy into the bandgap. For the parabola we also used the results of Kevan,[33] who found with high-resolution PES measurements a binding energy of this state at $\bar{X}$ of -0.06 eV and an effective mass of 0.07.

Our results for Cu(110) agree well with the results of Jacob *et al.*[5] and Bartynski *et al.*[25,34] At $\bar{Y}$ we used the PES results of Kevan,[35] who found an energy of -0.39 eV for the low-energy surface state at the zone boundary.

For Cu(111) our data agree well with Jacob *et al.*,[5] who measured only up to about 1.0 Å^{-1}. At $\bar{\Gamma}$ we used the PES result of Kevan[36] for the crystal induced surface state at -0.39 eV and an effective mass of 0.46. The structure at higher $k_{\parallel}$ for Cu(111) at about 1.3 Å^{-1} and 2–3 eV might also be a crystal-induced surface state at the zone boundary in analogy to the (100) and (110) surfaces, although the calculation with the combined-interpolation scheme also predicts a bulk transition close to the gap.

For Cu(110) and (111) at higher energy we find a bulk transition which can be triangulated in analogy to Ni.[37] For Cu(111) it can be seen only in the $\overline{\Gamma M}$ direction due to the initial-state effect discussed before, because the coupling of the initial-state wave function to the bulk states is different for $\overline{\Gamma M}$ and $\overline{\Gamma M'}$. This results in $\overline{\Gamma M'}$ direction in a total invisibility of this transition, although the matrix element is the same as in $\overline{\Gamma M}$ direction. In Fig. 5 the $E(k_{\parallel})$ dispersion of this bulk state for Cu(110) (squares) and on Cu(111) in $\overline{\Gamma M}$ direction (diamonds) is shown. The solid symbols are the experimental results. The open symbols are the results of the combined-interpolation-scheme calculation. The initial state of this transition has $(11\bar{1})$ character, whereas the final state is characterized by $(\bar{1}1\bar{1})$. The triangulation in the ΓXUL mirror plane is given in Fig. 6. The large arrows indicate the $k_{\parallel}$ directions for the (111) and (110) surfaces in the mirror plane, which are perpendicular to the corresponding surface normals marked as arrows. The triangulation is done in the following way: From Figs. 5 one extracts the $k_{\parallel}$ values for the (110) and (111) surfaces for the constant final-state energy (therefore the method is also called the energy-coincidence method). The intersection of the two (dashed) straight lines defined by the respective $k_{\parallel}$ values provides the desired k-space location of the observed transition and is shown as a solid diamond. The length of the symbols indicates the experimental error in triangulation, resulting from the error in the energy and $k_{\parallel}$. The error in the energy is shown in Fig. 5 by error

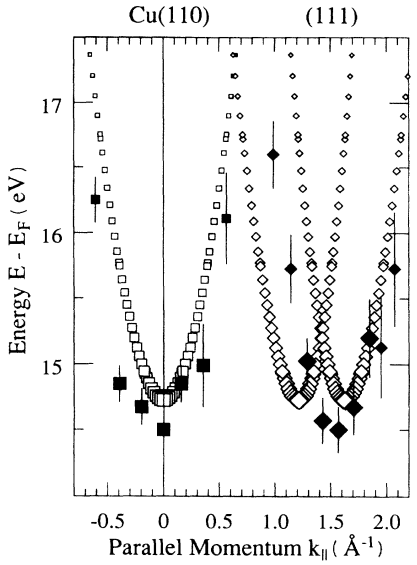

FIG. 5. $E(k_{\|})$ diagram for the higher-energy bulk transition, which can be seen for Cu(110) (squares) and Cu(111) (diamonds). The open symbols are the results of the combined interpolation scheme calculation, the solid symbols with error bars show our experimental data.

bars, whereas the error in $k_{\|}$ is 0.1 Å $^{-1}$ due to the limited angular resolution of the electron gun of $\pm 2°$. The experimental triangulation results show a good agreement with the results of the combined-interpolation scheme calculation (open diamonds). The $k_{\perp}$ of the incoming electron is changed by the surface in such a way that only the transition in the second Brillouin zone is observable as can be seen in Figs. 5 and 6. This transition, which can be seen for Cu(110) and (111), will be used in the next section to discuss the strong influence of surface effects for the temperature dependence of bulk transitions.

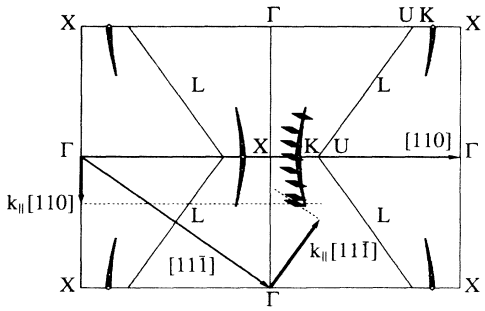

FIG. 6. Triangulation of the higher-energy bulk transition of Fig. 5 in the ΓXUL mirror plane. The large arrows indicate the $k_{\|}$ directions for the (110) and (111) surfaces in the mirror plane, which are perpendicular to the surface normals marked as arrows. The results of the combined interpolation-scheme calculation are shown as open diamonds. The experimental triangulation is done in the following way: From Fig. 5 one extracts the $k_{\|}$ values for the (110) and (111) surface for the same energy of the state. From these values one gets the experimental results as indicated by the dashed lines.

III. TEMPERATURE-DEPENDENT RESULTS FOR CU(100), (110), AND (111)

For the temperature-dependent measurements the photon takeoff angle was optimized for each transition to obtain maximum count rates.[14] Temperatures were measured by thermocouples which give an estimated uncertainty of 10 K for the values given in the following sections. Heating and cooling of the sample had no effect on the alignment within 0.5°. In Fig. 7 a typical set of temperature-dependent IPE measurements are shown. Both electron gun and photon detector lie in the ΓX mirror plane of the crystal. We use the convention that our angles of the electrons or photons are positive if the angle is counted clockwise from the surface normal to the position of the electron gun or the photon detector. If the signs of the angle of incidence of the electrons and the photon takeoff angle are different, the positions of the electron gun and the photon detector are on different sides of the surface normal.[14] The main temperature effect is the reduction of the intensities of the transitions with increasing temperature. The background, indicated by the dashed line in Fig. 7, is found to be independent of temperature within the statistical error limits. The peak width and shape also do not show a temperature dependence, although we must note here that our experimental setup is not able to detect small changes because of its limited resolution [full width at half maximum (FWHM), 0.7 eV].[38]

In the following, the peak intensities were measured as a function of temperature during cooling down after heating the sample to 900 K. Several independent runs were accumulated to reduce the statistical error. The intensities were corrected for the background. Possible bulk impurity segregation and contamination during the experiment could be excluded by the comparison of IPE spectra before and after the temperature-dependent measurements.

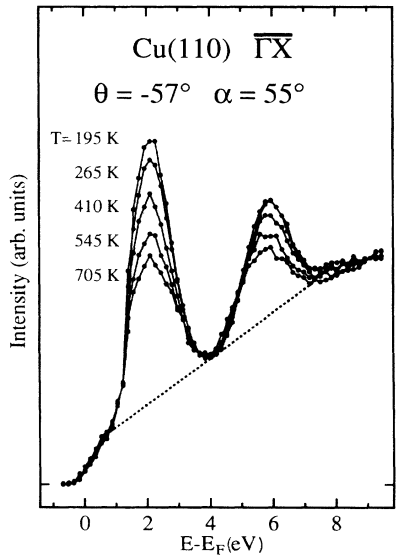

FIG. 7. Set of IPE spectra for Cu(110) for several temperatures. The background is indicated by the dashed line.

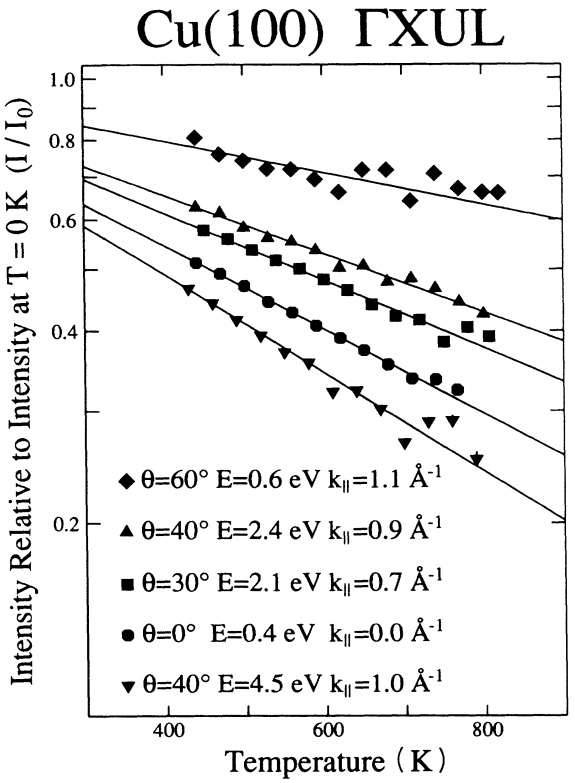

FIG. 8. Intensity of various inverse photoemission transitions for Cu(100) as a function of temperature.

A. Bulk transitions

Data for several transitions taken in the ΓXUL mirror plane on a Cu(001) surface are shown in Fig. 8. The data points are plotted semilogarithmically versus temperature and can be fitted well by straight lines. The statistical uncertainty is indicated by error bars, which are in most cases smaller than the size of the symbols. The normalization of the data points comes from the extrapolation of the straight line fits to $T=0$ K. The inverse gradient of the straight lines can be expressed as a characteristic temperature T_c representing the temperature interval over which the intensity drops by a factor $1/e$. The various transitions are characterized by the final-state energy E_f and by the parallel momentum $k_{\parallel}$ relative to the surface normal in the respective mirror planes. This information is sufficient to look up the transitions in the dispersion curves of Sec. II. The typical error for the characteristic temperatures of this work is 20 K.

The interpretation of the results can be made within a simple Debye-Waller ansatz[11]

$$I=I_0\exp(-\langle u^2\rangle\Delta\mathbf{k}^2)\ , \tag{3}$$

where $\langle u^2\rangle$ is the mean-square displacement of the atoms and $\Delta\mathbf{k}$ is the momentum exchanged in the transition. This result has been derived for transitions from d into free-electron-like bands in Ref. 11, but we will show in Sec. IV that it is also applicable for transitions between free-electron-like bands. The mean-square displacement is to a good approximation a linear function of temperature T and can be expressed in the Debye-model[39] as

$$\langle u^2\rangle=3\hbar^2T/(Mk_B\Theta_D^2)\ . \tag{4}$$

Here, M is the mass of the atom, Θ_D is the Debye temperature, and k_B is Boltzmann's constant. The combination of Eqs. (3) and (4) immediately gives the exponential decrease of the intensity with temperature as observed by the experiment (Fig. 8). The momentum $\Delta\mathbf{k}$ is obtained from the calculations with the combined interpolation scheme of Sec. II and by a comparison of the experimental data with the calculated bulk transitions in Figs. 2–5. This way we obtain the exchanged momentum $\Delta\mathbf{k}$ (in

TABLE I. Characteristic temperatures T_c determined from the experimental data for the temperature dependence of various bulk transitions. With the exchanged momentum $\Delta\mathbf{k}$ the Debye temperature θ_D can be calculated.

Mirror plane	Surface	θ	E (eV)	$k_{\parallel}$ (Å^{-1})	T_c (K)	$\Delta k/(\pi/a)$	θ_D (K)
ΓXUL	Cu(100)	0°	0.4	0	660	200	135
ΓXUL	Cu(100)	−30°	2.1	0.7	820	200	150
ΓXUL	Cu(100)	−40°	4.5	1.0	560	200	125
ΓXUL	Cu(100)	−40°	2.4	0.9	940	111	140
$\Gamma XUL\bar{\Gamma}\bar{M}'$	Cu(111)	−40°	0.9	0.8	1370	200	190
						111	170
$\Gamma XUL\bar{\Gamma}\bar{M}$	Cu(111)	−45°	1.1	0.9	1370	200	190
						111	170
$\Gamma XUL\bar{\Gamma}\bar{M}$	Cu(111)	−50°	14.0	1.7	670	200	150
ΓXUL	Cu(110)	0°	−0.5[a]	0	900–1000	220	240
ΓXUL	Cu(110)	−3°	14.0	0.1	870	200	190
ΓXWK	Cu(100)	0°	−0.2[b]	0	1050	200	170
ΓXWK	Cu(100)	0°	−1.2[b]	0	1020	200	170
ΓXWK	Cu(100)	−30°	1.5	0.6	1270	200	190
ΓXWK	Cu(100)	−50°	12.4	1.6	660	220	190
ΓXWK	Cu(110)	−57°	2.0	1.1	880	200	150

[a]Reference 3.
[b]Reference 1.

units of π/a, where a is the lattice constant) and with the aid of Eqs. (3) and (4) we can calculate the Debye temperatures. All data are summarized in Table I. For the low-energy transitions for Cu(111) two different possibilities for the momentum $\Delta\mathbf{k}$ are given, because this transition is a mixture of these two parts. For Cu(110) the data in Table I are derived from straight-line fits for a temperature range between 200 and 400 K for reasons, which will be discussed in the next section.

The results of PES for the temperature dependence of the intensity for free-electron-like band transitions[1,3] are also included in Table I. The data are based in this case on measurements on two or three different temperatures. We also corrected the PES data for the background in analogy to the IPE data.

The variation of the Debye temperatures in Table I is smaller than the scatter of the characteristic temperatures. This shows that the reduction of the experimental data with the momentum transfer $\Delta\mathbf{k}$ is correct for bulk transitions between nearly-free-electron bands.

One point remains, however, to be discussed. All Debye temperatures are considerably smaller than the bulk Debye temperature of 340 K.[40] In order to estimate surface Debye temperatures we have performed calculations for a 25 layer slab in the harmonic approximation with only nearest-neighbor interaction following Ref. 41 with the force constants from Cu(100),[42] Cu(110),[43] and Cu(111).[44] We calculated surface Debye temperatures of 246 K for Cu(100), 224 K for Cu(110), and 213 K for Cu(111).[45] Even correlated displacements do not bring the Debye temperature into the range of the experimental value of approximately 160 K. We therefore conclude that the temperature dependence of IPE is significantly influenced by multiple-scattering processes. This fact is well known from the dynamical analysis of low-energy electron diffraction (LEED) I-V data.[46] Multiple scattering is not included in the simple model of Eq. (3). The PES data from Ref. 1, with photon energies of 11 and 14 eV agree well with the IPE data, whereas the PES data from Ref. 3, with a photon energy of 45 eV gives a greater Debye temperature than the IPE data for a photon energy of 9.6 eV, thus indicating the importance of the photon energy. Perhaps, the higher photon energy of 45 eV results in smaller multiple scattering effects for the final photoemission state. From Fig. 8 and Table I we also see that the hand-waving argument, which suggests a greater temperature dependence for higher angles of incidence because of the higher surface sensitivity and the fact that surface atoms have higher mean-square displacements than bulk atoms, is in contradiction to the experimental observations.

A PES study on the temperature dependence of the intensity of transitions between free-electron-like bands on Ag(100) showed a stronger temperature dependence with increasing energy.[47] Our results are compatible with this observation.

The remaining question is whether the multiple-scattering processes occur mainly in the bulk or in the surface region. In Fig. 9(a) the temperature dependence of the direct transition into a bulk state, which has been triangulated from Cu(111) and (110) in Sec. II, is shown. We would expect the same temperature dependence for both surfaces if bulk effects are dominating the temperature dependence, because it is the identical bulk transition observed on different surfaces. The intensity for Cu(110) decreases much more strongly than for Cu(111). In Fig. 9(b) the data of Fig. 9(a) and for a bulk transition for Cu(100) are plotted semilogarithmically. The IPE data for Cu(100) and (111) can be fitted well by the straight lines, whereas the data for Cu(110) decrease above approximately 400 K stronger than the straight lines. This can be seen in Fig. 10, where the mean-square displacements calculated with the Debye-Waller ansatz of Eq. (3) for the IPE data are shown. The data for Cu(111) follow a linear dependence up to 800 K, whereas the data for Cu(110) deviate from that linear dependence above

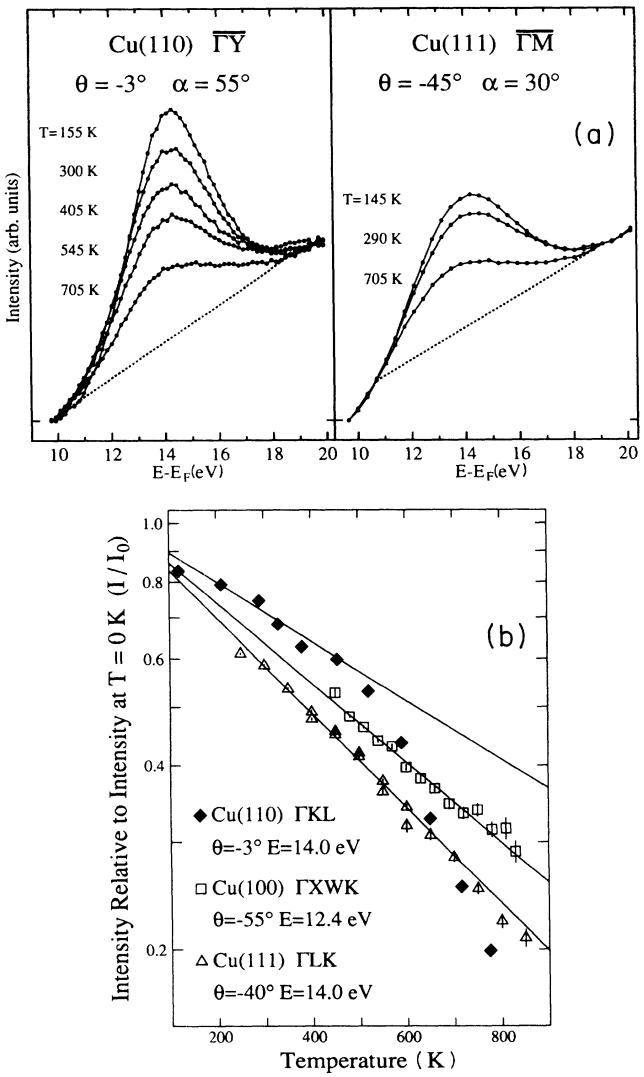

FIG. 9. (a) Inverse photoemission spectra for the same bulk transition observed on two different surfaces for various sample temperatures. (b) Semilogarithmic plot for the temperature dependence of the intensity of the transitions of (a) and of a bulk transition for Cu(100). The straight lines are linear fits for the temperature range from 200 to 900 K for Cu(111) and Cu(100) or to approximately 400 K for Cu(110).

400 K. Inspection of Fig. 10 shows a surprisingly good agreement between IPE and results from helium atom[48,49] and ion scattering.[50] The He atom scattering data are corrected for correlated vibrations following Ref. 48. For Cu(100) a deviation from the linear behavior above 800 K can be found. Unfortunately, we were not able to obtain IPE data in this temperature range because of rapid evaporation of copper onto the entrance window of the Geiger-Müller counter. We multiplied the IPE data for Cu(111) and (110) by a factor of 0.35 and for Cu(001), which is a different transition, by a factor of 0.75 in order to correct for multiple-scattering effects. By using the scaling factor for the triangulated transition as determined by comparison with the results of the scattering experiments on Cu(110), we find a very good agreement of the IPE data for Cu(111) with the mean-square displacements of surface atoms, derived from phonon slab calculations.[45] The deviation from the linear dependence may be due to the anharmonicity of the potential at the surface. This results in increased mean-square displacements at the surfaces of Cu(001) and (110) above 800 and 400 K, respectively. In our previous work[51] we interpreted the deviation of the temperature dependence of IPE for Cu(110) above 400 K from the expected linear behavior as an effect of the occurence of adatoms or defects on the surface, suggesting a roughening transition. This interpretation is at variance with Helium scattering experiments[49] which showed no indication of roughening up to 900 K for Cu(110). All experimental data confirm that up to 900 K at the most a few percent of adatoms exist.

Since the scattering experiments probe only the top surface layer, the good agreement shows conclusively that the temperature dependence of IPE is strongly influenced by vibrations of the atoms in the surface layer. We would like to note here that the mean free path of electrons in our energy range is about 10 Å (Ref. 52) corresponding to up to five layers. Surface-specific effects should be dominant only in the first two or three layers, with deeper layers showing essentially bulk behavior.

B. Transitions into surface states

The results for the transitions into surface states are summarized in Table II. The barrier-induced surface states show no temperature dependence, in full accord with expectation. In fact, their insensitivity to temperature variations was originally a means of identifying their character.[53] The crystal-induced surface states behave similarly to the bulk states. The temperature dependence of their intensity follows a Debye-Waller law for Cu(100) and (111), whereas for Cu(110) they show a stronger dependence above approximately 400 K (Fig. 11, data from Fig. 7.). The different behavior of these two kinds of surface states can be understood, because the barrier-induced image-potential surface states have wave functions with the highest probability outside the surface in the vacuum.[31] Both wave function and image-potential are quite insensitive to vibrations of the atoms at the surface or in the bulk. This explains the negligible temperature dependence observed in the experiment.[53] The crystal-induced surface states are sensitive to the potential at the surface and their wave functions have the highest probability at the surface.[31] Therefore, they should be very sensitive to vibrations at the surface and should show a strong temperature dependence.[5]

From Table II we can extract several trends for transitions into crystal-induced surface states. In analogy to bulk transitions, which can be triangulated, transitions into surface states for different surfaces, which are locat-

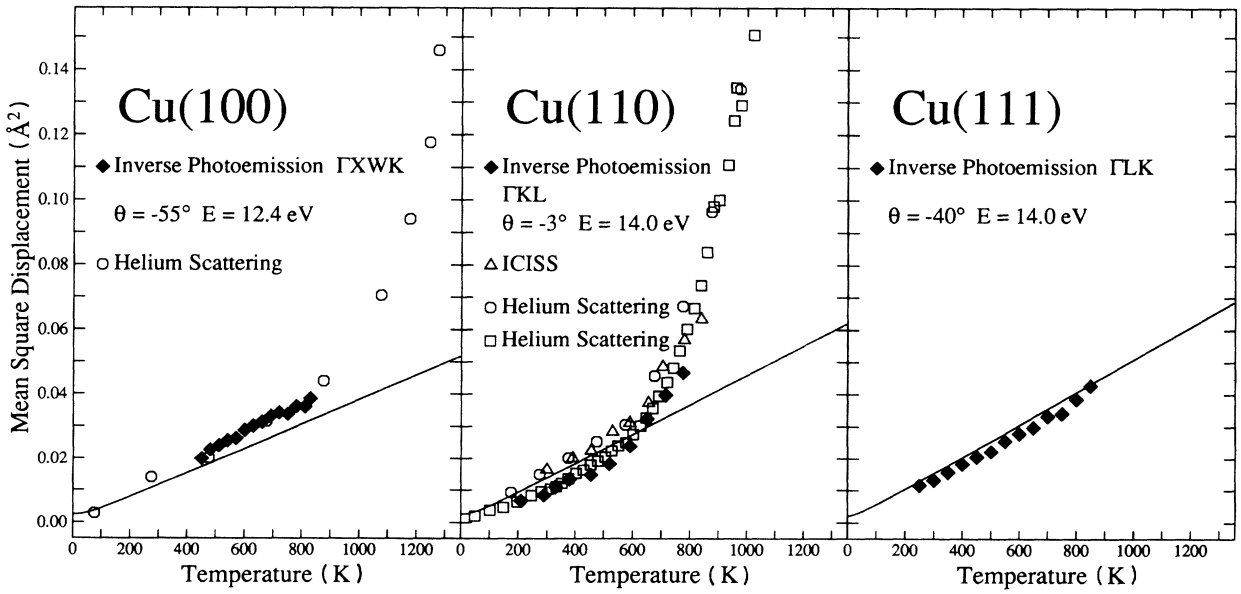

FIG. 10. Mean-square displacements of surface atoms as a function of temperature for the three low-index copper surfaces. The IPE data agree well with results from He atom (Refs. 48 and 49) and ion-scattering (Ref. 50) measurements. For higher temperatures a deviation from the phonon calculations is found for Cu(110) and Cu(100).

TABLE II. Characteristic temperatures T_c determined from the experimental data for the temperature dependence of various transitions into surface states. The band gaps, in which the surface states are located, are also listed.

Mirror plane	Surface	θ	E (eV)	$k_{\parallel}$ (Å^{-1})	T_c (K)	Band gap
		Barrier-induced surface states				
ΓXUL	Cu(100)	0°	4.1	0	$\geq 20\,000$	X_4'-X_1
ΓXUL	Cu(111)	0°	4.4	0	$\geq 30\,000$	L_2'-L_1
		Crystal-induced surface states				
ΓXUL	Cu(100)	−40°	3.8	1.0	840	L_2'-L_1
ΓXUL	Cu(100)	−60°	0.6	1.1	1750	L_2'-L_1
ΓXUL	Cu(110)	−32°	2.1	0.7	720	L_2'-L_1
ΓXUL	Cu(111)	0°	−0.3[a]	0	1800	L_2'-L_1
$\Gamma XUL\overline{\Gamma M}, \overline{\Gamma M}'$	Cu(111)	−15°	0.9	0.3	4700	L_2'-L_1
$\Gamma XUL\overline{\Gamma M}'$	Cu(111)	−60°	3.2	1.2	2140	X_4'-L_1
$\Gamma XUL\overline{\Gamma M}'$	Cu(111)	−70°	2.8	1.3	1400	X_4'-L_1
ΓXWK	Cu(110)	−57°	2.3	1.2	875	X_4'-X_1
ΓXWK	Cu(110)	−57°	5.6	1.4	940	X_4'-X_1

[a]Reference 1.

ed in the same band gap and have nearly the same relative position in it, show the same temperature dependence [e.g., in the L_2'-L_1 gap at 0.6 eV for Cu(001) and at −0.3 eV for Cu(110) (Ref. 1)].

The temperature dependence of the states with lower energy, which are closer to the band gap, is smaller than that of those with higher energy, which are further away from the band gap. Especially the measurements for Cu(111), which indicate a smaller temperature dependence the more bulk character the surface states accumulate. The "best" surface states are found in the center of the band gap. Near the border of the band gap or outside the band gap in the case of surface resonances the surface states pick up more and more bulk state character. This has also been measured in photoemission for a Tamm surface state for Ag(100),[47] which had close to the $\overline{M}$ point the highest-temperature dependence. Moving away from the zone boundary the temperature dependence decreased.

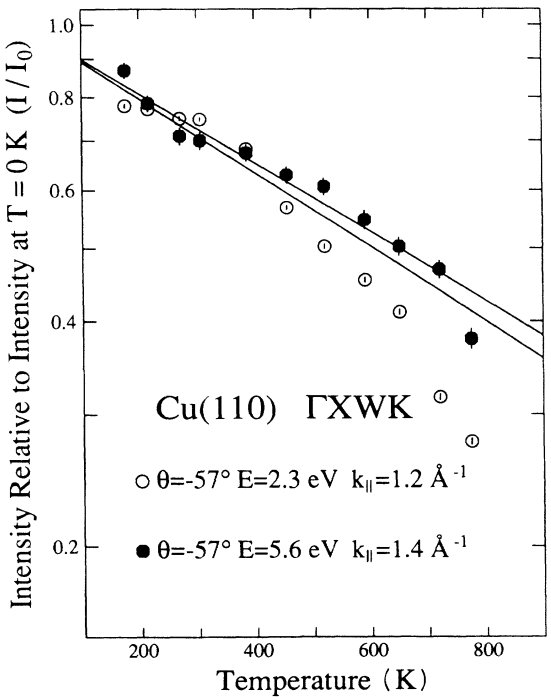

FIG. 11. Semilogarithmic plot of the temperature dependence of the intensity of the transitions of Fig. 7. The straight lines are linear fits for the temperature range from 200 to approximately 400 K.

IV. NFE THEORY AND TEMPERATURE EFFECTS

In PES most of the temperature-dependent measurements dealt with transitions from d into free-electron-like bands.[53] Shevchik[11] discussed the temperature effects for these kinds of transitions by describing the wave function of the d state with a tight-binding basis and that of the free-electron-like state with plane waves. By calculating the transition probability and introducing thermal vibrations from the lattice atoms he was able to show that for this kind of transition the temperature dependence of the intensity should follow the Debye-Waller form of Eq. (3). We have to note here, that for d bands due to their high localization, many reciprocal-lattice vectors can contribute to the momentum transfer, because the d bands have a very wide Fourier spectrum. The experimental results show no systematic behavior and disagree with this simple model and with one-step-model calculations. A possible explanation is a complicated coupling of the d orbitals caused by the thermal vibrations,[54] but up to now no realistic calculation exists.

In our IPE measurements of Sec. III the bulk transitions were all transitions between nearly-free-electron-like bands for which Shevchik's theory cannot be applied. In the following we will first show that Eq. (3) can be retrieved in the two-band approximation of the nearly-free-electron model. This result can then readily be extended to the full nearly-free-electron theory.

A. Two-band model

The simplest model to describe transitions between free-electron-like bands is the well-known two-band model,[20] which was discussed in Sec. II. In the two-band model the crystal potential is assumed to have only one Fourier component

$$V(\mathbf{r})=V_{\mathbf{G}}\exp(i\mathbf{G}\cdot\mathbf{r}) , \tag{5}$$

where $\mathbf{G}$ is the difference between the reciprocal-lattice vectors of the initial and final state.

For the discussion of the temperature effects in the crystal potential $V(\mathbf{r})$ the equilibrium position of an atom $\mathbf{r}_0$ is replaced by $\mathbf{r}_0+\mathbf{u}$, where $\mathbf{u}$ is the displacement of the atom due to the thermal vibrations. Power series expansion of Eq. (5) around $\mathbf{r}_0$ and time averaging (indicated by the angular brackets) gives

$$V_{\mathbf{G}}(T)=V_{\mathbf{G}}\exp[-0.5\langle(\mathbf{G}\cdot\mathbf{u})^2\rangle] . \tag{6}$$

We used the fact that all odd powers of $\mathbf{u}$ must be zero in the time average, because in the harmonic approximation for thermal vibrations the probability for $\mathbf{u}$ is equal to $-\mathbf{u}$. Otherwise, the equilibrium positions of the atom $\mathbf{r}_0$ must change.[40]

The temperature dependence of the expectation value of the momentum operator $\mathbf{p}$ is determined by combining Eq. (1) and (6)

$$\mathbf{p}(T)=\mathbf{p}\exp[-0.5\langle(\mathbf{G}\cdot\mathbf{u})^2\rangle] . \tag{7}$$

This allows for the temperature dependence of the intensity of direct transitions in the two-band model Eq. (3), because the intensity is proportional to the square of the expectation value of the momentum operator $\mathbf{p}$. Equation (7) shows that only the component of $\mathbf{u}$ in direction of the exchanged momentum $\mathbf{G}$, which is time independent, is relevant.

The substitution and time averaging is only correct for the final expressions of the expectation values of the observables to be discussed. Therefore one must be careful about the correct order of replacing the equilibrium positions of the atoms $\mathbf{r}_0$ by $\mathbf{r}_0+\mathbf{u}$, expanding around $\mathbf{r}_0$ and time averaging. Doing the time averaging in the individual wave functions $\psi_{i,f}=\sum_{\mathbf{k}} c_{\mathbf{k}_i,f}\exp(i\mathbf{k}_{i,f}\cdot\mathbf{r})$ gives Debye-Waller factors $\exp(-0.5\langle u^2\rangle\mathbf{k}_{i,f}^2)$ resulting in a different Debye-Waller factor for the momentum operator $\exp[-0.5(\mathbf{k}_i^2+\mathbf{k}_f^2)\langle u^2\rangle]$, which differs from the correct result of Eq. (7). The "phase information" between the Debye-Waller factors has been lost, as discussed before. Equations (3) and (7) show the importance of the coupling between the initial state and the final state by the direct transition.

We must note here that we neglect the thermal expansion of the lattice. This would result in Eqs. (1) and (6) in a temperature dependence of the reciprocal-lattice vector $\mathbf{G}$, because its unit (π/a) would become temperature dependent. For copper, the relative thermal expansion between room temperature and 800 K is 0.0094.[55] This would result in a 1% change of $\mathbf{G}$ and presumably also a negligible change in $V_{\mathbf{G}}$. This can be neglected compared with the large change in the mean-square displacements.

B. NFE theory

A more realistic treatment of free-electron-like bands is the extension of the basis of the two-band model to more plane waves with associated reciprocal-lattice vectors $\mathbf{G}_j$ and therefore more Fourier components $V_{\mathbf{G}_j}$ in the NFE theory.[39]

The temperature dependence is introduced in an analogy to the two-band model by

$$V_{\mathbf{G}_j}(T)=V_{\mathbf{G}_j}\exp[-0.5\langle(\mathbf{G}_j\cdot\mathbf{u})^2\rangle] . \tag{8}$$

We assume here that the Fourier coefficients $V_{\mathbf{G}_j}$ are independent from each other.

The transitions can now be influenced by more than only one Fourier component $V_{\mathbf{G}}$ and the temperature dependence is then determined by the different weights of the plane waves in the wave functions of the initial and the final state. Since the plane-wave coefficients depend on $k_{\parallel}$, a concomittant $k_{\parallel}$ dependence of the temperature effects is expected. Figure 12 shows the results of a NFE calculation for Cu(100) in the ΓXUL mirror plane for a

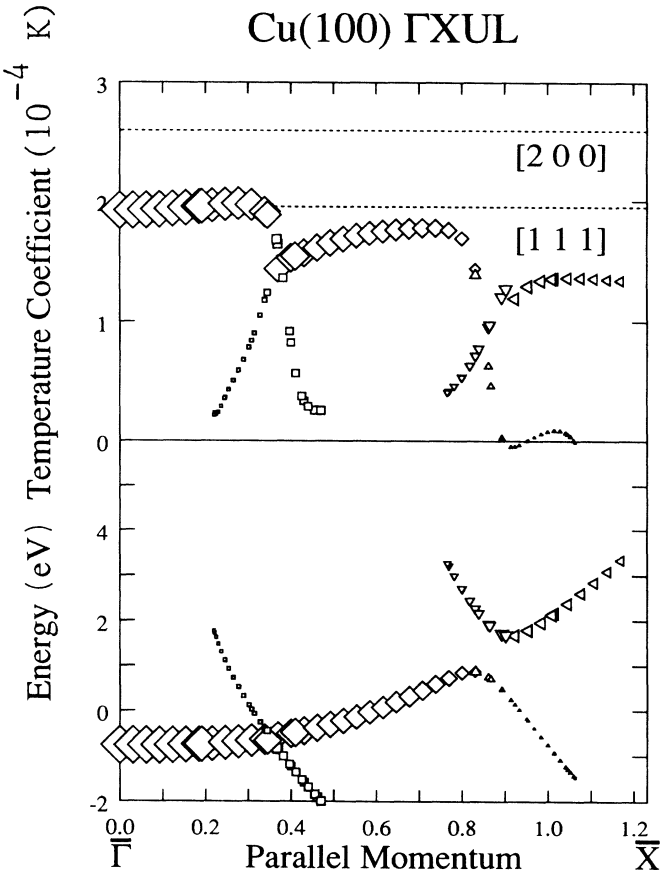

FIG. 12. NFE results for Cu(100) in the ΓXUL mirror plane. In the lower part the calculated possible transitions are shown, in the upper part the temperature coefficients, which are the inverse of the characteristic temperatures, for these transitions. The results of the simple two-band model for exchanged reciprocal-lattice vectors (200) and $(\bar{1}11)$ are shown as dotted lines.

photon energy of 9.6 eV. In the lower part the calculated possible transitions are shown, in the upper part the temperature coefficients which are the inverse of the characteristic temperatures for these transitions. We used the NFE parameters of the combined-interpolation-scheme calculation. The mean-square displacements were calculated within a Debye-model [Eq. (3)] with a Debye temperature of 340 K, which is the bulk value of copper. This value was used because we used a bulk model for bulk transitions. The results of the simple two-band model for exchanged reciprocal vectors (200) and (111) are shown as dotted lines. The (200) line should fit the temperature coefficient at normal incidence, whereas the (111) line should be equal to the zone-boundary value of the temperature coefficient, because there the wave functions of the states show nearly "pure" two-band character. The difference between the two-band model of Eq. (7) and the NFE calculation is due to thermal shifts of the states up to about 0.1 eV from 0 to 1000 K in the NFE calculation as a result of the temperature-dependent Fourier coefficients. The absolute values of the temperature coefficients from the NFE model are far away from the measured data. This discrepancy would be remedied by the choice of a smaller Debye temperature in the NFE calculations. This would lower the importance of the higher Fourier components compared to the lower ones, but it would not change the qualitative appearance of the curves in Fig. 12.

The comparison of Fig. 12 with Fig. 2 clearly shows that unfortunately for copper the free-electron-like bands are strongly influenced by hybridization with the *d* bands.[18] Therefore the NFE calculation is not able to reproduce the correct energy position. This hybridization is determined by the overlap integrals. Therefore, for a better description one would have to introduce the temperature effects into the combined-interpolation scheme. The problem is to describe the temperature dependence of the overlap integrals.

Also multiple-scattering effects are not included in these models. Therefore the absolute value of the calculated temperature coefficients are not significant. The general trend of the NFE calculation (see also Table III)—a decrease in the temperature coefficients with increasing energy—cannot be verified by our measurements. The nearly-free-electron model does not provide a proper description of temperature effects in IPE, despite the moderately successful classification of the observed bulk effects in terms of exchanged reciprocal-lattice vectors.

To make a more realistic description of the IPE spectra and to include multiple-scattering effects one can use the one-step model. This will be discussed in Sec. V.

V. ONE-STEP-MODEL CALCULATIONS

Following the ideas of Larsson and Pendry[12] we introduced the temperature effects into an existing one-step-model program.[56] The results of the phonon calculations[41] were used to introduce layer-dependent Debye temperatures, accounting for the enhanced vibrations of atoms at the surface. The results of temperature-dependent calculations for Cu(001) are shown in Fig. 13. We used the bulk and barrier parameters of Borstel and Thörner,[57] who were able to reproduce the measured IPE spectra. The bulk transitions show no temperature-dependent energy position, whereas the transitions into crystal-induced surface states show a shift to lower energy up to 0.15 eV, in agreement with previous work of Larsson and Pendry.[12] We have to note that we show the calculated data without accounting for the resolution of the experiment, which can be simulated by the convolution of the calculated data with a Gaussian of FWHM=0.7 eV. Therefore such shifts are difficult to detect in the experiment. We plot the calculated intensity for photons with the polarization vector **A** in the mirror plane. The intensity for photons with the polarization vector **A** perpendicular to the mirror plane gives for copper only an energy-independent contribution as shown for an angle of incidence for the electrons of 30°. The background shows only a very weak temperature dependence. This also holds for the transitions into barrier-induced surface states. The characteristic tem-

TABLE III. Characteristic temperatures T_c (Expt) determined from the experimental data for the temperature dependence of various bulk transitions and transitions into surface states. The one-step model of inverse photoemission and NFE theory can be used to calculate the characteristic temperatures T_c (one step) and T_c (NFE) directly.

Mirror plane	Surface	θ	E (eV)	$k_{\parallel}$ (Å^{-1})	T_c (K) (Expt)	T_c (K) (one step)	T_c (K) (NFE)
			Bulk transitions				
ΓXUL	Cu(100)	0°	0.4	0	660	1800	5000
ΓXUL	Cu(100)	−30°	2.1	0.7	820	1550	5600
ΓXUL	Cu(100)	−40°	4.5	1.0	560	1400	9100
ΓXUL	Cu(100)	−40°	2.4	0.9	940	1750	9500
ΓXUL	Cu(111)	−50°	14.0	1.7	670	450	8330
ΓXUL	Cu(110)	−3°	14.0	0.1	870	450	8330
			Transitions into surface states				
ΓXUL	Cu(100)	−40°	3.8	1.0	840	650	
ΓXUL	Cu(100)	−60°	0.6	1.1	1750	2000	

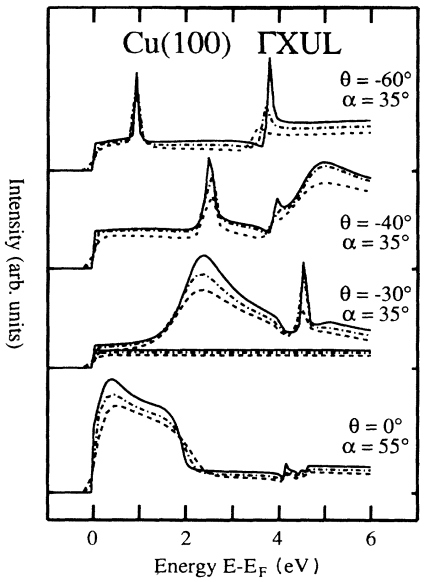

FIG. 13. Temperature-dependent one-step-model calculations for Cu(100) ΓXUL. The solid, dash-dotted, and dashed lines correspond to $T=0$, 300, and 800 K.

peratures extracted from our calculations with background correction are compared in Table III with the experimental results. Excluding the value for normal incidence for Cu(100) the experimental results fit the trend that the temperature dependence is stronger with increasing energy as expected from the one-step model, where the temperature dependence of IPE is mainly determined by the scattering of the initial state. We have to note that for normal incidence for Cu(100) the temperature dependence of the bulk state at 0.4 eV might also be influenced by the crystal-induced surface state at 1.1 eV, which can be seen as a shoulder in the spectrum.[30] The discrepancies in the absolute values between theory and experiment for the characteristic temperatures are not so surprising, because of the approximation of the distribution functions of the displacements of the atoms by δ functions and because of the neglect of correlations and electron-phonon coupling in the one-step model.[12] We would like to point out that the one-step model is not able to reproduce Eq. (3), which is the correct result for two physically meaningful cases for transitions from localized d states[11] and free-electron-like states into free-electron-like bands. This suggests the inadequacy of some approximations in the temperature-dependent one-step model.

VI. CONCLUSIONS

The temperature dependence of the intensities of direct transitions in IPE is influenced significantly by multiple-scattering processes in the surface region. It is determined by surface vibrations and by the exchanged momentum $\Delta\mathbf{k}$ for bulk transitions between nearly-free-electron bands as expected from NFE and two-band-model calculations. Unfortunately, these calculations are not able to reproduce the results from experiment in more detail.

For Cu(100) and (111) the temperature dependence can be fit very well with a Debye-Waller law, where the mean-square displacements of the surface atoms increase linearly with temperature. For Cu(110) we find an enhancement of the mean-square displacements above 400 K in agreement with other scattering experiments.

The one-step model of photoemission and the results of phonon calculations for surface vibrations have been combined to give a theoretical description of the measured temperature dependencies. The results are not quite satisfying, although they seem to show the right trend: the stronger the temperature dependence is the greater the energy is.

The transitions into barrier-induced surface states show within the experimental error limits no temperature dependence in accord with expectation.[53]

The crystal-induced surface states are sensitive to the potential at the surface and their wave functions have the highest probability at the surface. Therefore they respond sensitively to vibrations at the surface and show a strong temperature dependence. Transitions into states which are located in the same band gap and have nearly the same relative position in it, show the same temperature dependence. The temperature dependence gets smaller the more bulklike the surface state becomes.

The temperature dependence of IPE can be interpreted in the following picture: In an observed direct transition in IPE, the incoming electron couples to the initial bulk state and decays to the final state by producing a photon. The temperature introduces vibrations of the lattice atoms. Therefore, the increased scattering of electrons out of the initial state by the vibrating atoms with increasing temperature is the dominant temperature-dependent process and results in a decrease of the intensity of the transition. Since the radiative transition is fast compared to the lattice vibrations, they take place in a quasistatic distorted lattice. The fact that initial and final state experience the same lattice distortions is reflected by the importance of the exchanged momentum. The scattered electrons can decay to lower energies also via processes producing the background in the IPE spectra. The background is mainly determined by radiative transitions after electron-hole pair production. The decreasing intensity of the direct transition need not result in an observable increase in the background, because in the decay of the scattered electron via a direct transition of different photon energy the electron is not detected and in the decay via processes producing the background of the IPE spectra the gain of intensity for the background is distributed over the whole solid angle of 4π.

The temperature effects in photoemission spectroscopies appears to be a very complicated problem for realistic calculations. The treatment of PES or IPE for a realistic lattice with thermal vibrations under consideration for correlation effects and electron-phonon coupling is not possible at present, because the system loses its symmetry. For the discussion of temperature effects in photoemission spectroscopies due to other effects like structural phase transitions, thermal vibrations must always be included in the discussion. Finally, the existence

of temperature-dependent intensity variations on a nonmagnetic material like copper clearly underlines the extreme difficulty for isolating and interpreting temperature-dependent effects of magnetic origin for nickel. For nickel, the results for the nonmagnetic temperature effects should be transferable from copper, because the same transitions can be observed for both materials, only shifted in the energetic position.

[1]J. A. Knapp, F. J. Himpsel, A. R. Williams, and D. E. Eastman, Phys. Rev. B **19**, 2844 (1979).

[2]R. C. White, C. S. Fadley, M. Sagurton, P. Roubin, D. Chandresis, J. Lecante, C. Guillot, and Z. Hussain, Solid State Commun. **59**, 633 (1986).

[3]R. S. Williams, P. S. Wehner, J. Stöhr, and D. A. Shirley, Phys. Rev. Lett. **39**, 302 (1977).

[4]J. Württenberg, Ph.D. thesis, University Frankfurt (Main), 1987 (unpublished).

[5]W. Jacob, V. Dose, U. Kolac, Th. Fauster, and A. Goldmann, Z. Phys. B **63**, 459 (1986).

[6]H. Martensson, P.-O. Nilsson, and J. Kanski, Appl. Surf. Sci. **11/12**, 652 (1982).

[7]R. Drube, V. Dose, H. Derks, and W. Heiland, Surf. Sci. **214**, L253 (1989).

[8]M. Donath, Appl. Phys. A **49**, 351 (1989).

[9]R. Courths and S. Hüfner, Phys. Rep. **112**, 53 (1984), and references therein.

[10]A. Baalmann, M. Neumann, W. Braun, and W. Radlik, Solid State Commun. **54**, 583 (1985).

[11]N. J. Shevchik, Phys. Rev. B **16**, 3428 (1977); J. Phys. C **10**, L555 (1977); Phys. Rev. B **20**, 3020 (1979).

[12]C. Larsson and J. B. Pendry, J. Phys. C **14**, 3089 (1981).

[13]V. Dose, Appl. Phys. **14**, 117 (1977).

[14]Th. Fauster, R. Schneider, and H. Dürr, Phys. Rev. B **40**, 7981 (1989).

[15]Th. Fauster, Vacuum **38**, 129 (1988).

[16]R. Schneider, H. Dürr, Th. Fauster, and V. Dose, J. Vac. Sci. Technol. (to be published).

[17]N. V. Smith, Phys. Rev. B **19**, 5019 (1979).

[18]H. Bross and B. Schiekel (private communication).

[19]J. Hermanson, Solid State Commun. **22**, 9 (1977).

[20]N. V. Smith, Rep. Prog. Phys. **51**, 1227 (1988), and references therein.

[21]A. Goldmann, Vakuum-Technik **31**, 204 (1982).

[22]D. P. Woodruff, N. V. Smith, P. D. Johnson, and W. A. Royer, Phys. Rev. B **26**, 2943 (1982).

[23]R. Schneider, H. Dürr, Th. Fauster, and V. Dose, Vacuum (to be published).

[24]M. Donath, M. Glöbl, B. Senftinger and V. Dose, Solid State Commun. **60**, 237 (1986).

[25]R. A. Bartynski and T. Gustafsson, Phys. Rev. B **33**, 6588 (1986).

[26]V. Dose, Surf. Sci. Rep. **5**, 337 (1985).

[27]D. Straub and F. J. Himpsel, Phys. Rev. B **33**, 2256 (1986).

[28]N. G. Stoffel, W. A. Royer, and N. V. Smith, Phys. Rev. B **31**, 6815 (1985).

[29]N. V. Smith, Phys. Rev. B **32**, 3549 (1985).

[30]G. Thörner, G. Borstel, V. Dose, and J. Rogozik, Surf. Sci. **157**, L379 (1985).

[31]P. M. Echenique and J. B. Pendry, J. Phys. C **11**, 2065 (1978).

[32]S. L. Hulbert, P. D. Johnson, M. Weinert, and R. F. Garrett, Phys. Rev. B **33**, 760 (1986).

[33]S. D. Kevan, Phys. Rev. B **28**, 2268 (1983).

[34]R. A. Bartynski, T. Gustafsson, and P. Soven, Phys. Rev. B **31**, 4745 (1985).

[35]S. D. Kevan, Phys. Rev. B **28**, 4822 (1983).

[36]S. D. Kevan, Phys. Rev. Lett. **50**, 526 (1983).

[37]A. Goldmann, M. Donath, W. Altmann, and V. Dose, Phys. Rev. B **32**, 837 (1985).

[38]V. Dose, Th. Fauster, and R. Schneider, Appl. Phys. A **40**, 203 (1986).

[39]N. W. Ashcroft and N. D. Mermin, *Solid State Physics* (Holt Saunders, London, 1976).

[40]C. Kittel, *Introduction to Solid State Physics* (Wiley, New York, 1971).

[41]S. Lehwald, F. Wolf, H. Ibach, B. M. Hall, and D. L. Mills, Surf. Sci. **192**, 131 (1987).

[42]M. Wuttig, R. Franchy, and H. Ibach, Solid State Commun. **57**, 445 (1986).

[43]P. Zeppenfeld, K. Kern, R. David, K. Kuhnke, and G. Comsa, Phys. Rev. B **38**, 12329 (1989).

[44]J. E. Black, F. C. Shanes and R. F. Wallis, Surf. Sci. **133**, 199 (1983).

[45]H. Dürr, R. Schneider, and Th. Fauster (unpublished).

[46]J. B. Pendry, *Low Energy Electron Diffraction* (Academic, London, 1974).

[47]H. Martensson, P.-O. Nilsson, Surf. Sci. **152/153**, 189 (1985).

[48]D. Gorse and J. Lapujoulade, Surf. Sci. **162**, 847 (1985).

[49]P. Zeppenfeld, K. Kern, R. David, and G. Comsa, Phys. Rev. Lett. **62**, 63 (1989).

[50]H. Dürr, R. Schneider, and Th. Fauster, Vacuum (to be published).

[51]Th. Fauster, R. Schneider, H. Dürr, G. Engelmann, and E. Taglauer, Surf. Sci. **189/190**, 610 (1987).

[52]G. Ertl and J. Küppers, *Low Energy Electrons and Surface Chemistry* (Verlag Chemie, Weinheim, 1974).

[53]V. Dose, W. Altmann, A. Goldmann, U. Kolac, and J. Rogozik, Phys. Rev. Lett. **52**, 1919 (1984).

[54]H. Martensson, C. G. Larsson, and P.-O. Nilsson, Surf. Sci. **126**, 214 (1983).

[55]*American Institute of Physics Handbook* (McGraw-Hill, New York, 1972).

[56]J. F. L. Hopkinson, J. B. Pendry, and D. J. Titterington, Comput. Phys. Commun. **19**, 69 (1980).

[57]G. Borstel and G. Thörner, Surf. Sci. Rep. **8**, 1 (1987).

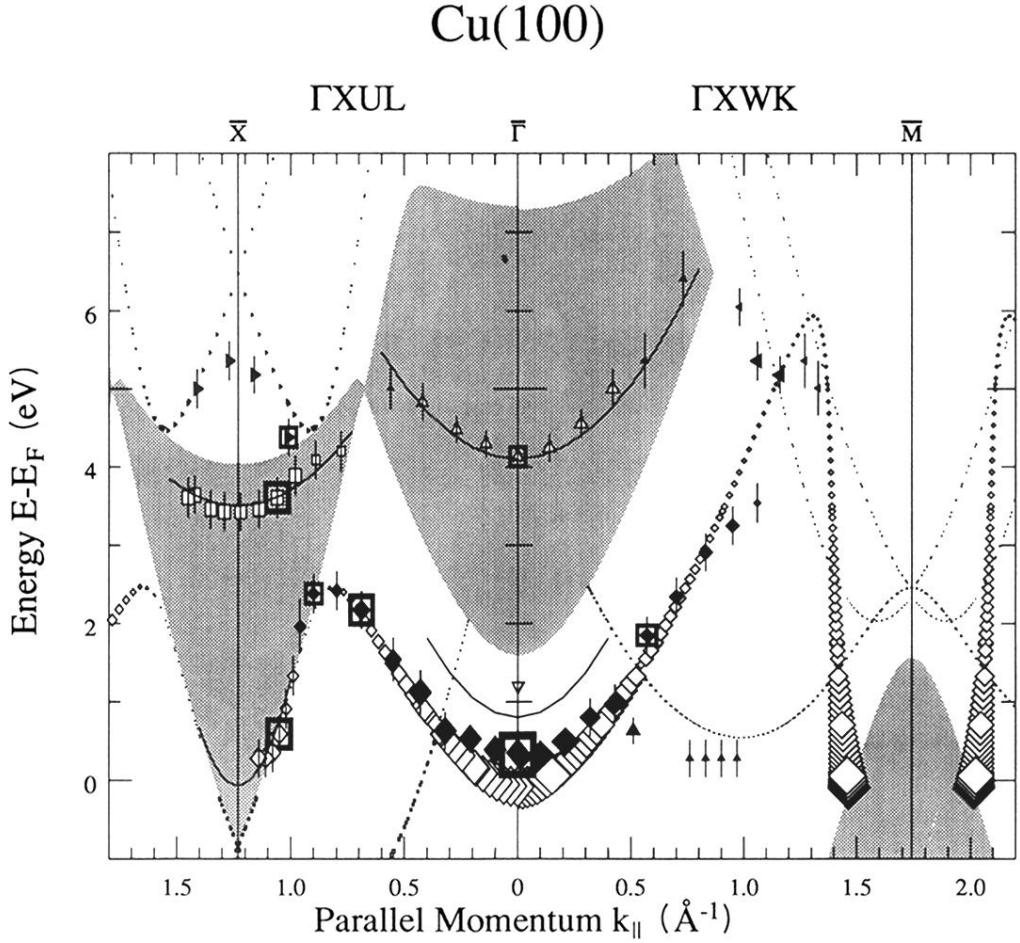

FIG. 2. $E(k_{\parallel})$ diagram for Cu(100). The calculated transitions are shown by the open symbols without error bars corresponding to Fig. 1. The data from our measurements for bulk transitions are shown as solid symbols with error bars. The size of the symbols indicates the intensity of the transition. The symbols of the measured bulk transitions were chosen to correspond to the calculated transitions. The band gaps of the projected bulk band structure are shown as grey shaded areas. The data from our measurements for transitions into surface states are marked as open symbols with error bars. The dispersion of the surface states is indicated by the parabolas.

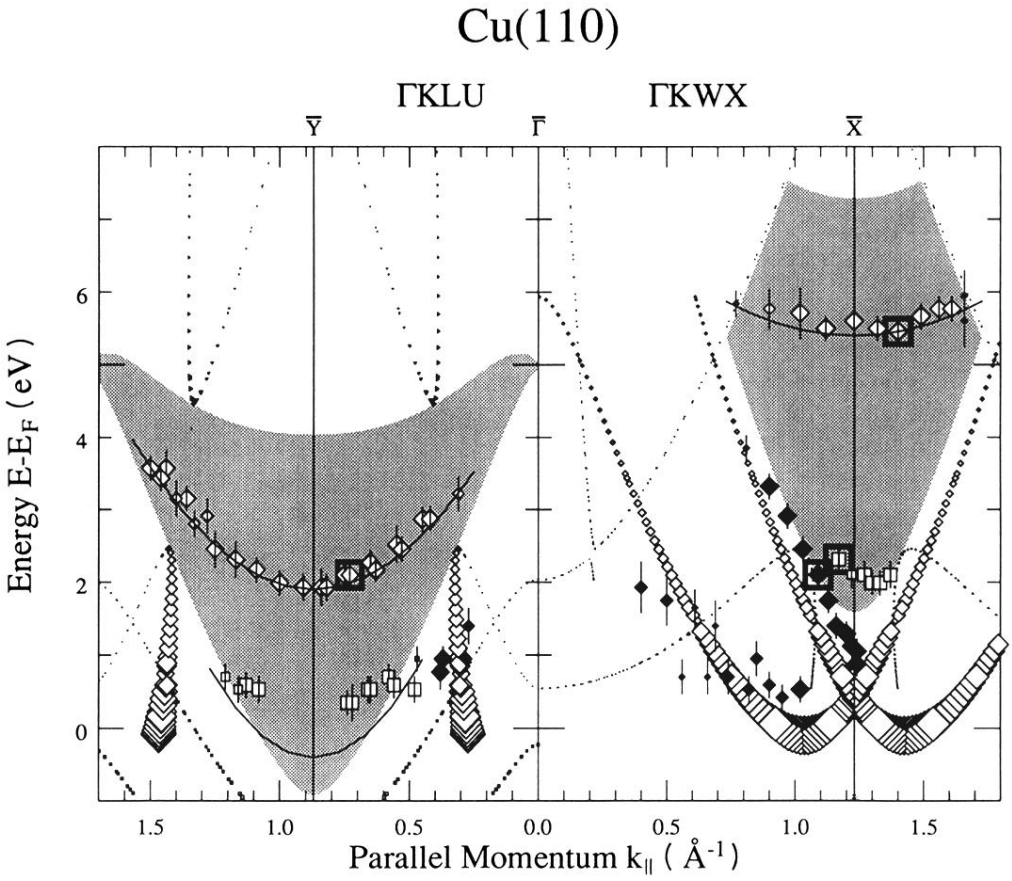

FIG. 3. $E(k_{\|})$ diagram for Cu(110). For an explanation see Fig. 2.

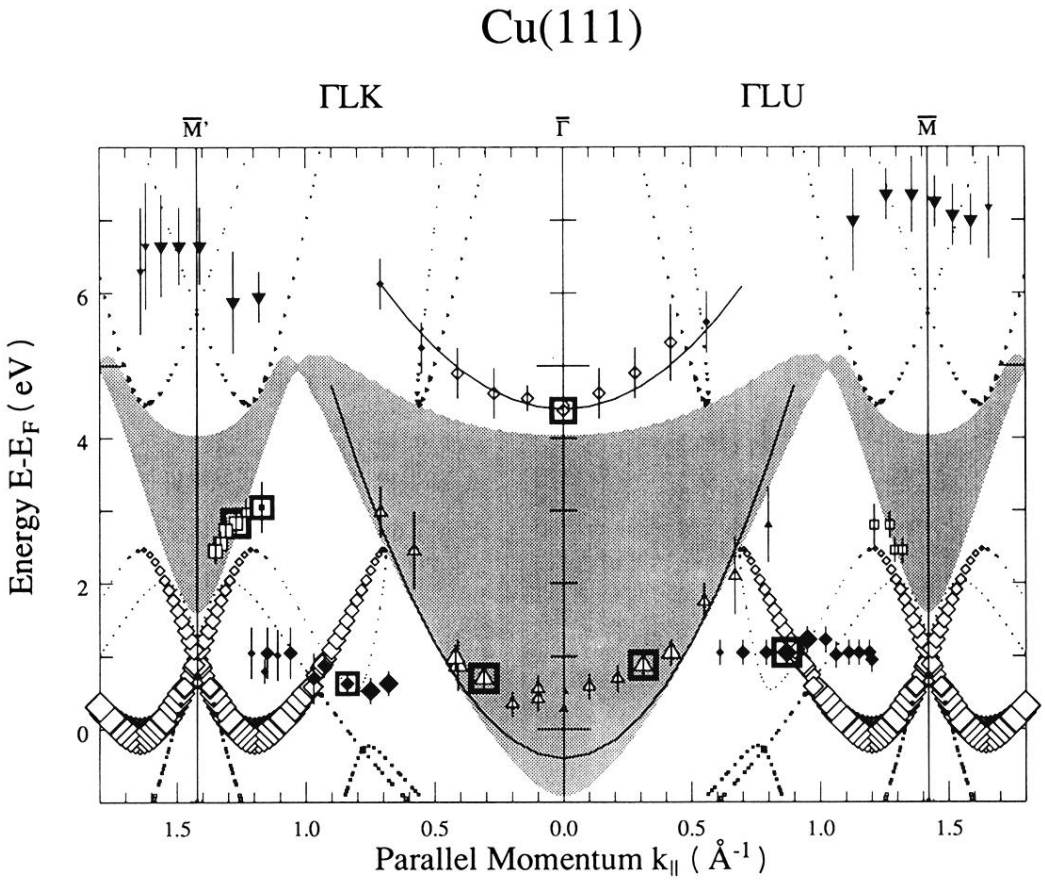

FIG. 4. $E(k_{\parallel})$ diagram for Cu(111). For an explanation see Fig. 2.